ARTICLE

doi:10.1038/nature13109

C11orf95–RELA fusions drive oncogenic NF-κB signalling in ependymoma

Matthew Parker[1,2]*, Kumarasamypet M. Mohankumar[3]*, Chandanamali Punchihewa[4]*, Ricardo Weinlich[5]*, James D. Dalton[1,4], Yongjin Li[1,2], Ryan Lee[4], Ruth G. Tatevossian[1,4], Timothy N. Phoenix[3], Radhika Thiruvenkatam[3], Elsie White[3], Bo Tang[1,4], Wilda Orisme[1,4], Kirti Gupta[4], Michael Rusch[2], Xiang Chen[2], Yuxin Li[2,6], Panduka Nagahawhatte[2], Erin Hedlund[2], David Finkelstein[2], Gang Wu[2], Sheila Shurtleff[4], John Easton[1,4], Kristy Boggs[1], Donald Yergeau[1], Bhavin Vadodaria[1], Heather L. Mulder[1], Jared Becksfort[2], Pankaj Gupta[2], Robert Huether[6], Jing Ma[1], Guangchun Song[1], Amar Gajjar[1,7], Thomas Merchant[8], Frederick Boop[9], Amy A. Smith[10], Li Ding[1,11,12], Charles Lu[1,11], Kerri Ochoa[1,11,12], David Zhao[1,2], Robert S. Fulton[1,11], Lucinda L. Fulton[1,11,12], Elaine R. Mardis[1,11,12,13], Richard K. Wilson[1,11,12,13], James R. Downing[1,4], Douglas R. Green[5], Jinghui Zhang[1,2], David W. Ellison[1,4] & Richard J. Gilbertson[1,3]

Members of the nuclear factor-κB (NF-κB) family of transcriptional regulators are central mediators of the cellular inflammatory response. Although constitutive NF-κB signalling is present in most human tumours, mutations in pathway members are rare, complicating efforts to understand and block aberrant NF-κB activity in cancer. Here we show that more than two-thirds of supratentorial ependymomas contain oncogenic fusions between *RELA*, the principal effector of canonical NF-κB signalling, and an uncharacterized gene, *C11orf95*. In each case, *C11orf95–RELA* fusions resulted from chromothripsis involving chromosome 11q13.1. C11orf95–RELA fusion proteins translocated spontaneously to the nucleus to activate NF-κB target genes, and rapidly transformed neural stem cells—the cell of origin of ependymoma—to form these tumours in mice. Our data identify a highly recurrent genetic alteration of *RELA* in human cancer, and the C11orf95–RELA fusion protein as a potential therapeutic target in supratentorial ependymoma.

Ependymomas are tumours of the brain and spinal cord[1]. Surgery and irradiation remains the mainstay of treatment of this disease as chemotherapy is ineffective in most patients. Consequently, ependymoma is incurable in up to 40% of cases[2].

Although ependymomas from the different regions of the central nervous system (CNS) are histologically similar, they possess site-specific prognoses, transcriptional profiles and DNA copy number alterations[3–7], suggesting that they are different diseases that are likely to require different treatments. We recently generated the first mouse model of supratentorial ependymoma by amplifying *EPHB2*—a common DNA copy number alteration of these tumours—in mouse forebrain neural stem cells (NSCs)[6]. Preclinical studies using this model have identified new treatments that are now in clinical trial[8]. Drugs that target genetic alterations in the other types of ependymoma could provide new therapies, but the identity of these alterations remains largely unknown.

The *C11orf95–RELA* translocation

To identify additional genetic alterations that drive ependymoma, we carried out whole-genome sequencing (WGS) of 41 tumours and matched normal blood, and RNA sequencing (RNA-seq) of the transcriptomes of 77 tumours (Fig. 1, Extended Data Fig. 1 and Supplementary Tables 1–3).

Single nucleotide variations, insertion/deletions, and focal copy number variations (less than five genes) were rare in ependymomas, but structural variations were detected relatively frequently[9], especially in supratentorial tumours (median structural variations, supratentorial tumours = 23 versus posterior fossa tumours = 7.5, $P = 0.0006$, Wilcoxon ranked sum test; Extended Data Fig. 2a, b, Supplementary Information, Supplementary Figs 1–7 and Supplementary Tables 4–11). All nine supratentorial ependymomas analysed by WGS contained structural variations that clustered within chromosome 11q12.1–11q13.3, producing catastrophic disruption of the locus and an oscillating copy number state compatible with chromothripsis (chromosome 11: 50–60 Mb, $FWER = 9.6 \times 10^{-5}$ and chromosome 11: 60–70 Mb, $FWER = 7.8 \times 10^{-7}$, Mann–Whitney test; Fig. 1, Extended Data Fig. 2c, Supplementary Information and Supplementary Table 12)[10]. Although the chromothripsis region differed in each tumour, eight of the nine cases shared a common region (~63 to ~67 Mb) in which the reordered chromosome fragments fused a poorly characterized gene, *C11orf95*, to *RELA*, the principal effector of canonical NF-κB signalling[11,12] (Extended data Figs 3 and 4a, b). These genes are normally separated by 1.9 Mb containing 73 genes (Extended Data Fig. 4a, Supplementary Figs 8–10 and Supplementary Tables 1 and 13). The *C11orf95–RELA* translocation was validated in all eight cases by independent orthogonal sequencing and interphase fluorescence *in situ* hybridization (FISH) using 'break-apart' probes to *C11orf95* and *RELA* (Fig. 1, Extended Data Fig. 4c, Methods, Supplementary Figs 8 and 9, and Supplementary Tables 14 and 15). In marked contrast, neither chromothripsis nor *C11orf95–RELA* translocations

[1]St. Jude Children's Research Hospital - Washington University Pediatric Cancer Genome Project, Memphis, Tennessee 38105, USA. [2]Department of Computational Biology and Bioinformatics, St. Jude Children's Research Hospital, Memphis, Tennessee 38105, USA. [3]Department of Developmental Neurobiology, St. Jude Children's Research Hospital, Memphis, Tennessee 38105, USA. [4]Department of Pathology, St. Jude Children's Research Hospital, Memphis, Tennessee 38105, USA. [5]Department of Immunology, St. Jude Children's Research Hospital, Memphis, Tennessee 38105, USA. [6]Structural Biology, St. Jude Children's Research Hospital, Memphis, Tennessee 38105, USA. [7]Department of Oncology, St. Jude Children's Research Hospital, Memphis, Tennessee 38105, USA. [8]Department of Radiological Sciences, St. Jude Children's Research Hospital, Memphis, Tennessee 38105, USA. [9]Department of Surgery, St. Jude Children's Research Hospital, Memphis, Tennessee 38105, USA. [10]MD Anderson Cancer Center Orlando, Pediatric Hematology/Oncology, 92 West Miller MP 318, Orlando, Florida 32806, USA. [11]The Genome Institute, Washington University School of Medicine in St Louis, St Louis, Missouri 63108, USA. [12]Department of Genetics, Washington University School of Medicine in St Louis, St Louis, Missouri 63108, USA. [13]Siteman Cancer Center, Washington University School of Medicine in St Louis, St Louis, Missouri 63108, USA.

*These authors contributed equally to this work.

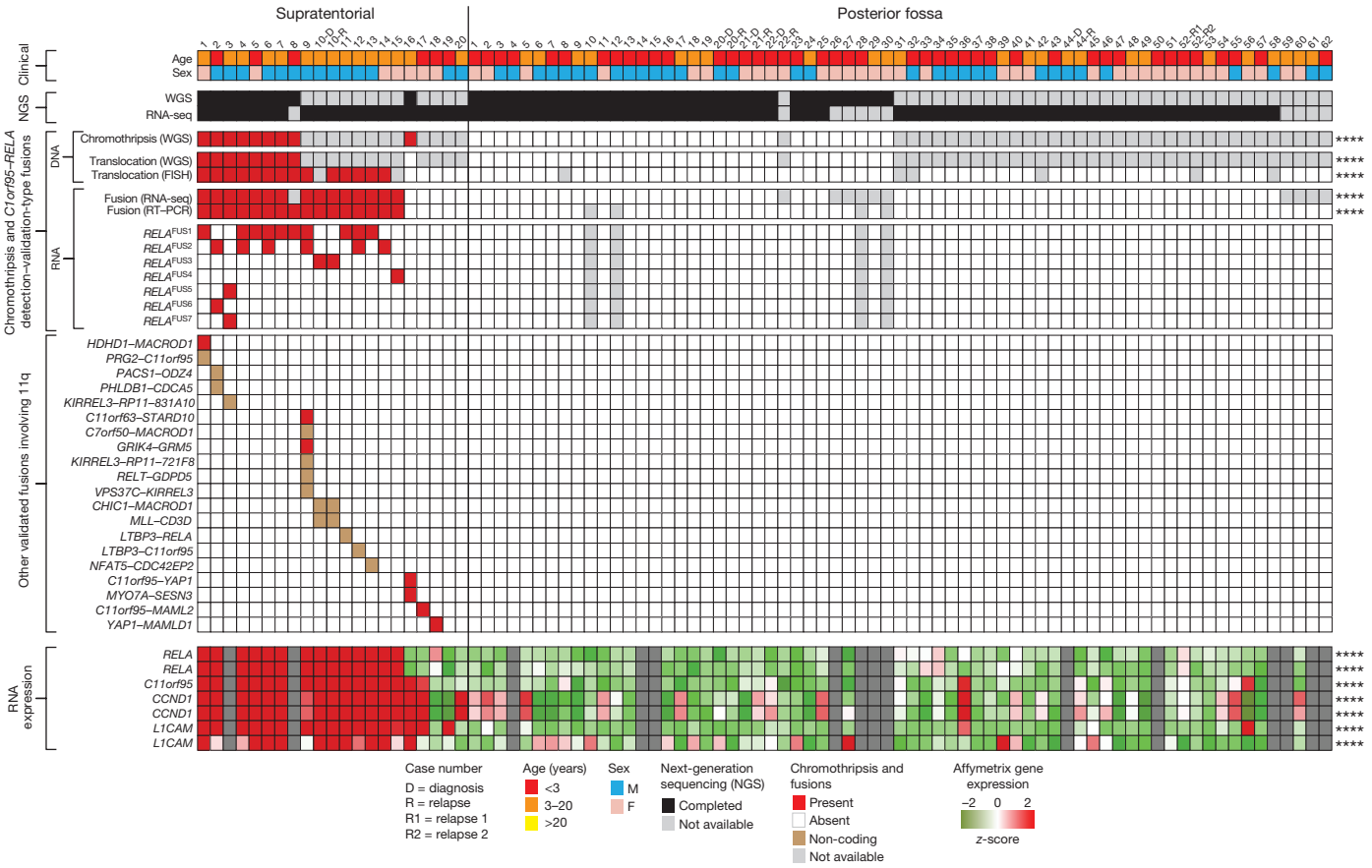

Figure 1 | Recurrent *C11orf95–RELA* translocations in human supratentorial ependymoma. Summary of results of molecular assays of translocations in tumours from 82 patients with ependymoma (****$P < 0.0001$ Fisher's exact test for supratentorial versus posterior fossa tumour). 'RNA expression' at bottom reports Affymetrix array data (****$Q < 0.0001$ for supratentorial versus posterior fossa tumour).

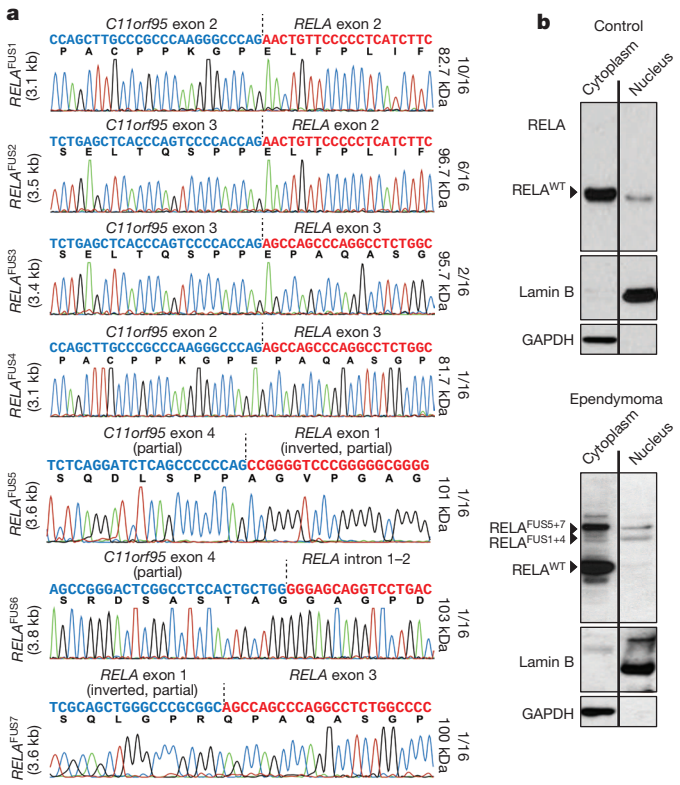

were detected in any of the 32 posterior fossa tumours analysed by WGS ($P < 0.0001$, Fisher's exact test).

Next, using a novel algorithm, we looked for *C11orf95–RELA* fusion transcripts in the 77 ependymomas analysed by RNA-seq (Fig. 1 and Supplementary Methods). Fusion transcripts were validated by polymerase chain reaction with reverse transcription (RT–PCR) and Sanger sequencing (Fig. 2a and Extended Data Fig. 5a). *C11orf95–RELA* transcripts were detected in all eight supratentorial tumours in which the translocation was detected by WGS (Fig. 1 and Supplementary Table 16a). Fusion transcripts were also detected in an additional seven supratentorial tumours: FISH detected the *C11orf95–RELA* translocation in six of these with available material (Fig. 1). *C11orf95–RELA* transcripts were not detected in supratentorial tumours that lacked the translocation or in any posterior fossa ependymomas (Fig. 1; $P < 0.0001$, Fisher's exact test).

Translocation-positive tumours contained mature, spliced, in-frame fusion transcripts together with premature fusion transcripts containing intronic or intergenic DNA breakpoints (Fig. 2a and Extended Data Figs 4c and 6; see also Supplementary Information and Supplementary Fig. 10 for details of all fusion breakpoints). Thus, splicing is required to generate mature *C11orf95–RELA* transcripts. Seven distinct, mature *C11orf95–RELA* fusion transcripts were observed (Fig. 2a and Extended Data Fig. 5b). The most frequent (which we refer to here as *RELA*^{FUS1})

Figure 2 | *C11orf95–RELA* fusion transcripts and proteins. **a**, Electropherograms of seven distinct *RELA* fusion transcripts detected in ependymoma. The proportion of tumours containing the corresponding fusion transcript, and the predicted protein product size are shown on the right. **b**, Western blot analysis of RELA proteins in cytoplasmic and nuclear extracts of 'control' human 293T cells (top) and supratentorial ependymoma ST3 (bottom).

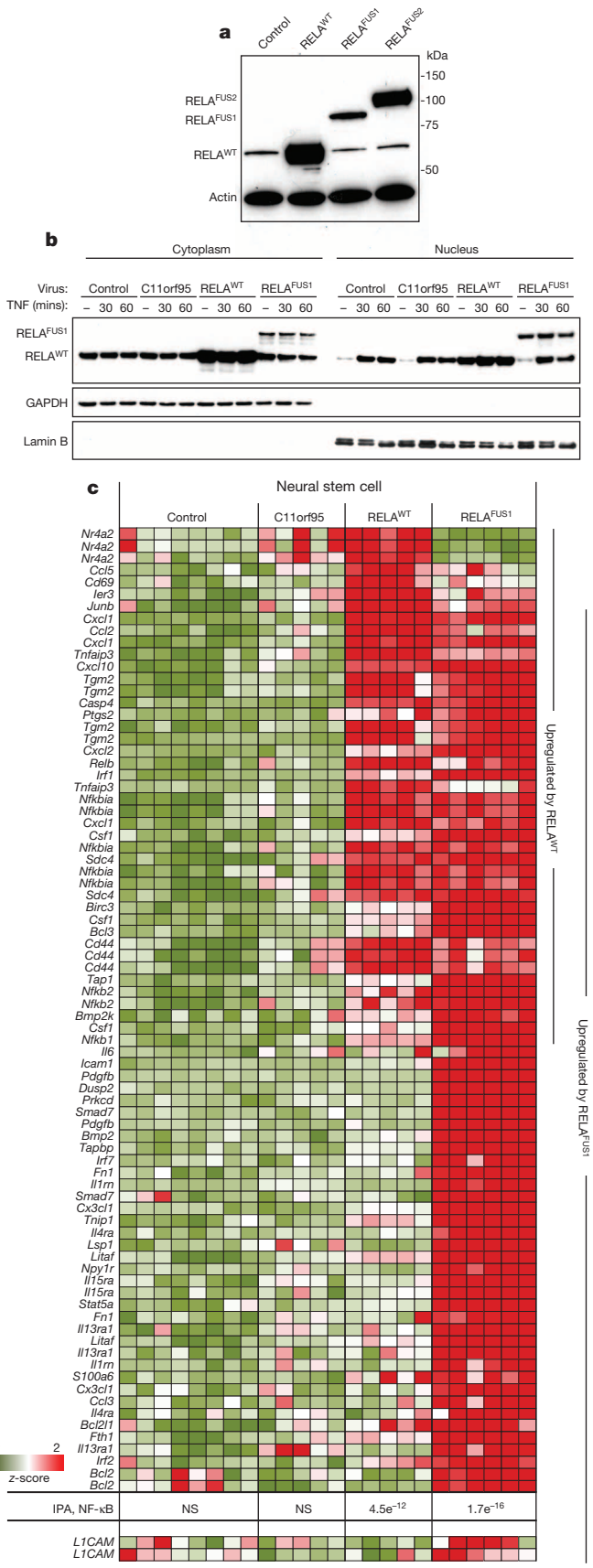

Figure 3 | Cell trafficking and transcriptional activity of wild-type and fusion RELA proteins. **a**, RELA western blot analysis of 293T cells transduced with the indicated retroviruses. **b**, Western blot analysis of RELA proteins in cytoplasmic and nuclear extracts of 293T cells transduced with the indicated virus, treated with TNF (50 ng ml^{-1}). **c**, Expression of NF-κB target genes upregulated in mouse NSCs transduced by the indicated retrovirus. *P* value of NF-κB pathway activation detected by IPA and expression of L1CAM are shown at the bottom (see Methods for sources of target genes). NS, not significant.

included exons 1 and 2 of *C11orf95* and, except for the first two codons, the entire open reading frame of *RELA* (Figs 1 and 2a). Six other fusion transcripts (*RELA*^{FUS2}–*RELA*^{FUS7}) were detected less frequently, but each was observed in tumours lacking *RELA*^{FUS1}, suggesting that they may be oncogenic.

Western blot analysis detected wild-type RELA (RELA^{WT}) protein in supratentorial ependymoma ST3 (supratentorial 3) and human control (293T) cells (Fig. 2b). ST3, but not control cells, also expressed at least four RELA proteins that corresponded to the appropriately sized products of fusion transcripts detected in this tumour by RNA-seq and RT–PCR (Figs 1 and 2b, and Extended Data Fig. 6). RELA fusion and RELA^{WT} proteins segregated differently in ST3 cells, with fusion products accumulating preferentially in the nucleus relative to the wild-type protein.

To validate further the *C11orf95–RELA* translocation we analysed a separate cohort of 89 formalin-fixed paraffin-embedded (FFPE) ependymomas using FISH and RT–PCR (Extended Data Fig. 7 and Supplementary Table 1). FISH detected the *C11orf95–RELA* translocation in 67% ($n = 14$ of 21) of primary FFPE supratentorial ependymomas, but in none of 64 posterior fossa tumours, and RT–PCR confirmed the presence of fusion transcripts exclusively in translocation-positive tumours ($P < 0.0001$ Fishers exact test; Extended Data Fig. 7a).

These data identify *C11orf95–RELA* translocations as the most recurrent genetic alteration in ependymoma, affecting approximately 70% of supratentorial tumours ($n = 29$ of 41) and occurring preferentially in older patients (mean age translocation-positive, translocation-negative supratentorial tumours = 8.3 ± 0.9 years, 3.5 ± 1.7 years, respectively; $P < 0.05$, Mann–Whitney test, Fig. 1). We are currently interrogating a larger cohort of supratentorial ependymomas to assess the prognostic significance of the *C11orf95–RELA* translocation.

RNA-seq identified 20 other fusion transcripts involving chromosome 11q (Fig. 1, Supplementary Fig. 11 and Supplementary Table 16b, c). Thirteen of these occurred in tumours containing *C11orf95–RELA* and are predicted to be non-coding, suggesting they are 'passenger' events. However, four of seven 'coding' fusion transcripts occurred in ependymomas that lacked a *C11orf95–RELA* translocation. Two of these fused *C11orf95* to alternative transcriptional regulators: *C11orf95–YAP1* and *C11orf95–MAML2* (Fig. 1 and Extended Data Fig. 5b). Thus, the zinc finger domains of C11orf95 are likely to be essential oncogenic elements of these fusions, possibly altering the trafficking, degradation or target specificity of partner transcription factors.

C11orf95–RELA drives NF-κB signalling

Members of the NF-κB family of transcriptional regulators are central mediators of the cellular inflammatory response[13]. Although constitutive NF-κB signalling is present in most human tumours, mutations in pathway members are rare, complicating efforts to understand and block aberrant NF-κB activity in cancer[14–16]. We therefore examined whether C11orf95–RELA fusions drive aberrant NF-κB signalling in ependymoma.

RNA-seq and Affymetrix gene expression profiling detected increased expression of *C11orf95* and *RELA* in translocation-positive ependymomas, as well as high levels of CCND1—a direct transcriptional target of NF-κB signalling[17,18]—and L1CAM that is associated with aberrant cell–cell adhesion, invasion and NF-κB activation in tumours[19,20] ($Q < 0.0001$; Fig. 1). CCND1 and L1CAM protein expression were also strongly associated with the *C11orf95–RELA* translocation in FFPE supratentorial ependymomas ($P < 0.0001$, Fisher's exact test; Extended Data Fig. 7a, b). Upstream stimuli, for example, tumour necrosis factor (TNF), activate the NF-κB pathway by causing RELA-containing heterodimers to translocate to the nucleus and drive gene transcription[13].

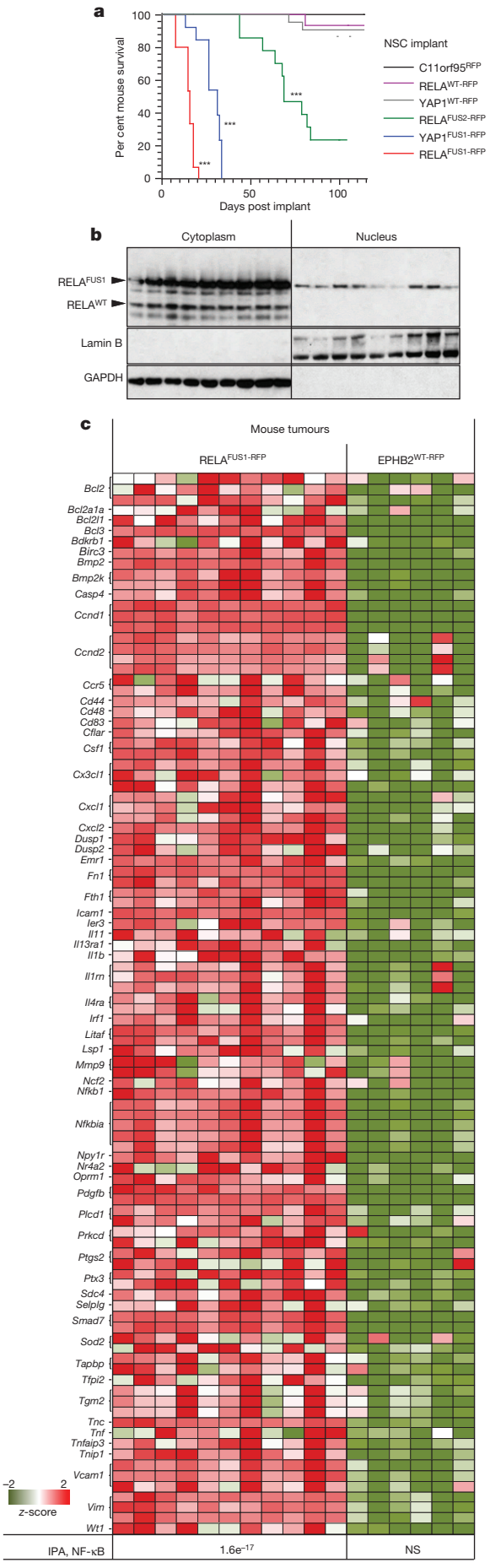

Figure 4 | *C11orf95–RELA* and *C11orf95-YAP1* fusions drive brain tumorigenesis. **a**, Survival curves of mice implanted with the indicated NSCs. (***$P < 0.0001$, log-rank test relative to control NSCs.) **b**, Western blot analysis of RELA proteins in cytoplasmic and nuclear extracts of nine independent mouse $RELA^{FUS1\text{-}RFP}$ brain tumours. **c**, Expression of NF-κB target genes significantly upregulated in $RELA^{FUS1\text{-}RFP}$ relative to $EPHB2^{WT\text{-}RFP}$ brain tumours. Bottom, *P* value of NF-κB activation detected by IPA.

However, RELA fusion proteins seem to accumulate preferentially in the nucleus of ependymoma cells relative to $RELA^{WT}$ protein (Fig. 2b). Therefore, we examined RELA protein trafficking in cells engineered to express exogenous C11orf95, $RELA^{WT}$ or $RELA^{FUS1}$ (Fig. 3a). As expected, endogenous $RELA^{WT}$ was sequestered in the cytoplasm of unstimulated control and C11orf95-transduced cells, but translocated to the nucleus to activate an NF-κB transcriptional reporter after exposure to TNF (Fig. 3b and Extended data Fig. 8). Conversely, overexpression of $RELA^{WT}$ resulted in spontaneous nuclear translocation and NF-κB transcription, supporting the idea that high levels of wild-type RELA can overwhelm the IκB inhibitory system[21]. Therefore, we titrated down the expression of the $RELA^{FUS1}$ fusion to approximate that of endogenous $RELA^{WT}$. Even at this reduced level, $RELA^{FUS1}$ translocated spontaneously to the nucleus and activated NF-κB transcription (Fig. 3b and Extended data Fig. 8).

We next investigated whether C11orf95–RELA drives an aberrant NF-κB transcriptional program in mouse NSCs that we have shown previously serve as cells-of-origin of ependymoma[6] (Fig. 3c). Neither control nor C11orf95 transduction altered gene expression in NSCs; but exogenous $RELA^{WT}$ upregulated 20% ($n = 25$ of 129) of a series of validated NF-κB target genes in NSCs, and ingenuity pathway analysis (IPA) confirmed highly significant activation of NF-κB signalling in these cells (IPA $P = 4.5 \times 10^{-12}$; Supplementary Information and Supplementary Table 17). Expression of $RELA^{FUS1}$ produced even greater activation of NF-κB target genes in NSCs, and also upregulated L1cam (IPA, $P = 1.7e^{-16}$; Fig. 3c, Supplementary Fig. 12 and Supplementary Table 17). Although L1CAM has been reported to activate NF-κB signalling in tumours[16,17], our NSC and tumour data suggest that it may itself be a target of aberrant C11orf95–RELA signalling (Figs 1 and 3c, and Extended Data Fig. 7b). $RELA^{FUS1}$ had a profound impact on the expression of several other genes that regulate focal adhesion, compatible with the notion that aberrant NF-κB signalling disrupts cell–cell adhesion in cancer[13,19] ($Q = 1.5 \times 10^{-10}$; Supplementary Table 18b).

C11orf95–RELA drives ependymoma

To test the transforming capacity of RELA fusion proteins, we isolated NSCs from *Ink4a/Arf*-null *Blbp–eGFP* (enhanced green fluorescent protein) transgenic mice as described previously[6], and transduced these with either C11orf95–red fluorescence protein ($C11orf95^{RFP}$), $RELA^{WT\text{-}RFP}$, $RELA^{FUS1\text{-}RFP}$ or $RELA^{FUS2\text{-}RFP}$ retroviruses. To begin to understand the relevance of the other fusions detected in ependymoma we also transduced NSCs with C11orf95–YAP1 ($YAP1^{FUS\text{-}RFP}$), or wild-type YAP1 ($YAP1^{WT\text{-}RFP}$). NSCs (1.5×10^6 RFP^+ NSCs) transduced with each virus were implanted separately into the cerebrum of 15 female 6-week-old CD1-nude mice. $C11orf95^{RFP}$, $RELA^{WT\text{-}RFP}$, or $YAP1^{WT\text{-}RFP}$ NSCs formed very few or no brain tumours in mice (median follow up 155 days; Fig. 4a). In marked contrast, all mice implanted with $RELA^{FUS1\text{-}RFP}$ NSCs succumbed within 20 days to brain tumours that recapitulated the 'clear cell' and finely branched vasculature characteristic of 'vascular-variant' human supratentorial ependymoma[22] ($P < 0.0001$ log-rank test; Fig. 4a and Extended Data Fig. 7b). Similar to their human counterpart, mouse $RELA^{FUS1}$ ependymomas expressed nuclear phospho-Ser276-RELA that is indicative of, and required for, RELA transcriptional activity[23–25], as well as CCND1 and L1CAM (Extended Data Fig. 7a, b). Consistent with the human disease, nuclei of mouse $RELA^{FUS1}$ ependymomas also accumulated

RELA^{FUS1} protein relative to the wild-type protein (Figs 2b and 4b, and Extended Data Fig. 7b). RELA$^{FUS2\text{-}RFP}$ NSCs also generated tumours, albeit with a lower penetrance ($n = 10$ of 15 mice) and longer latency (median survival 68 days) than RELA$^{FUS1\text{-}RFP}$ NSCs, potentially explaining the biased selection of RELA^{FUS1} versus RELA^{FUS2} in human ependymomas. YAP1$^{FUS\text{-}RFP}$ NSCs formed brain tumours with high efficiency, indicating that other ependymoma translocations are oncogenic (Fig. 4a).

Finally, to determine whether C11orf95–RELA drives a specific, oncogenic NF-κB transcription program, we compared the transcriptomes of mouse RELA$^{FUS1\text{-}RFP}$ brain tumours with those of our supratentorial ependymoma mouse model driven by *EPHB2* (ref. 6). RELA$^{FUS1\text{-}RFP}$ mouse brain tumours displayed marked upregulation of NF-κB target genes (IPA, $P = 1.6e^{-17}$; Fig. 4c and Supplementary Fig. 13). Conversely, EPHB2$^{WT\text{-}RFP}$ mouse ependymomas expressed much lower levels of phospho-Ser276-RELA, L1CAM and CCND1 proteins and lacked NF-κB signal activation. Thus, *C11orf95–RELA* translocations are potent oncogenes that most probably transform NSCs by driving an aberrant NF-κB transcription program.

Aberrant NF-κB signalling is an established driver of solid tumours, but genetic evidence of pathway involvement has been lacking. We identify a highly recurrent genetic alteration that activates *RELA*, the principal effector of canonical NF-κB signalling, in human cancer. Furthermore, we show that C11orf95 is likely to be an essential partner in these translocations, possibly disrupting the cell trafficking of RELA and other partner transcription factors. We are currently investigating the mechanism by which RELA fusion proteins transform NSCs, and their potential to serve as a therapeutic target.

METHODS SUMMARY

Human tumour and matched blood samples were obtained with informed consent using an protocol approved by the institutional review board at St. Jude Children's Research Hospital. WGS, RNA-seq and analysis of all sequence data were performed as described previously[26]. Details of sequence coverage, custom capture and other validation procedures are provided in Supplementary Information (Supplementary Tables 2–6). Interphase FISH, immunohistochemistry of human and mouse tissues, western blot analysis, and RT–PCR were performed using standard techniques as described (Methods). Human and mouse messenger RNA profiles were generated using Affymetrix U133 2.0 and 430v2 arrays, respectively (Methods). NSCs were isolated and transduced with indicated retro- and lentiviruses in stem cell cultures as described previously[4,6,27] (see also Supplementary Information). All mouse studies were conducted according to protocols approved by the St. Jude Children's Research Hospital Animal Care and Usage Committee. NSCs were implanted under stereotactic control into the forebrain of immunocompromised mice and tumour growth monitored clinically and by bioluminescence[8]. All mouse brains were inspected by macroscopic dissection post-mortem. Fresh tumour cells were recovered from mouse brains as described previously[6].

Online Content Any additional Methods, Extended Data display items and Source Data are available in the online version of the paper; references unique to these sections appear only in the online paper.

Received 25 June 2013; accepted 28 January 2014.
Published online 19 February 2014.

1. Kleihues, P. *et al.* The WHO classification of tumors of the nervous system. *J. Neuropathol. Exp. Neurol.* **61,** 215–225; discussion 226–219 (2002).
2. Merchant, T. E. *et al.* Conformal radiotherapy after surgery for paediatric ependymoma: a prospective study. *Lancet Oncol.* **10,** 258–266 (2009).
3. Modena, P. *et al.* Identification of tumor-specific molecular signatures in intracranial ependymoma and association with clinical characteristics. *J. Clin. Oncol.* **24,** 5223–5233 (2006).
4. Taylor, M. D. *et al.* Radial glia cells are candidate stem cells of ependymoma. *Cancer Cell* **8,** 323–335 (2005).
5. Puget, S. *et al.* Candidate genes on chromosome 9q33–34 involved in the progression of childhood ependymomas. *J. Clin. Oncol.* **27,** 1884–1892 (2009).
6. Johnson, R. A. *et al.* Cross-species genomics matches driver mutations and cell compartments to model ependymoma. *Nature* **466,** 632–636 (2010).
7. Witt, H. *et al.* Delineation of two clinically and molecularly distinct subgroups of posterior fossa ependymoma. *Cancer Cell* **20,** 143–157 (2011).
8. Atkinson, J. M. *et al.* An integrated *in vitro* and *in vivo* high-throughput screen identifies treatment leads for ependymoma. *Cancer Cell* **20,** 384–399 (2011).
9. Wang, J. *et al.* CREST maps somatic structural variation in cancer genomes with base-pair resolution. *Nature Methods* **8,** 652–654 (2011).
10. Stephens, P. J. *et al.* Massive genomic rearrangement acquired in a single catastrophic event during cancer development. *Cell* **144,** 27–40 (2011).
11. Nolan, G. P., Ghosh, S., Liou, H. C., Tempst, P. & Baltimore, D. DNA binding and IκB inhibition of the cloned p65 subunit of NF-κB, a *rel*-related polypeptide. *Cell* **64,** 961–969 (1991).
12. Hansen, S. K., Baeuerle, P. A. & Blasi, F. Purification, reconstitution, and I kappa B association of the c-Rel-p65 (RelA) complex, a strong activator of transcription. *Mol. Cell. Biol.* **14,** 2593–2603 (1994).
13. DiDonato, J. A., Mercurio, F. & Karin, M. NF-κB and the link between inflammation and cancer. *Immunol. Rev.* **246,** 379–400 (2012).
14. Perkins, N. D. The diverse and complex roles of NF-κB subunits in cancer. *Nature Rev. Cancer* **12,** 121–132 (2012).
15. Baud, V. & Karin, M. Is NF-κB a good target for cancer therapy? Hopes and pitfalls. *Nature Rev. Drug Discov.* **8,** 33–40 (2009).
16. Chaturvedi, M. M., Sung, B., Yadav, V. R., Kannappan, R. & Aggarwal, B. B. NF-κB addiction and its role in cancer: 'one size does not fit all'. *Oncogene* **30,** 1615–1630 (2011).
17. Guttridge, D. C., Albanese, C., Reuther, J. Y., Pestell, R. G. & Baldwin, A. S. NF-κB controls cell growth and differentiation through transcriptional regulation of cyclin d1. *Mol. Cell. Biol.* **19,** 5785–5799 (1999).
18. Hinz, M. *et al.* NF-κB function in growth control: regulation of cyclin d1 expression and G0/G1-to-S-phase transition. *Mol. Cell. Biol.* **19,** 2690–2698 (1999).
19. Kiefel, H., Pfeifer, M., Bondong, S., Hazin, J. & Altevogt, P. Linking L1CAM-mediated signaling to NF-κB activation. *Trends Mol. Med.* **17,** 178–187 (2011).
20. Kiefel, H. *et al.* EMT-associated up-regulation of L1CAM provides insights into L1CAM-mediated integrin signalling and NF-κB activation. *Carcinogenesis* **33,** 1919–1929 (2012).
21. Courtois, G. & Gilmore, T. D. Mutations in the NF-κB signaling pathway: implications for human disease. *Oncogene* **25,** 6831–6843 (2006).
22. Godfraind, C. *et al.* Distinct disease-risk groups in pediatric supratentorial and posterior fossa ependymomas. *Acta Neuropathol.* **124,** 247–257 (2012).
23. Chen, L.-F. & Greene, W. C. Shaping the nuclear action of NF-κB. *Nature Rev. Mol. Cell Biol.* **5,** 392–401 (2004).
24. Zhong, H., Voll, R. E. & Ghosh, S. Phosphorylation of NF-κB p65 by PKA stimulates transcriptional activity by promoting a novel bivalent interaction with the coactivator CBP/p300. *Molecular Cell* **1,** 661–671 (1998).
25. Okazaki, T. *et al.* Phosphorylation of serine 276 is essential for p65 NF-κB subunit-dependent cellular responses. *Biochem. Biophys. Res. Commun.* **300,** 807–812 (2003).
26. Zhang, J. *et al.* The genetic basis of early T-cell precursor acute lymphoblastic leukaemia. *Nature* **481,** 157–163 (2012).
27. Robinson, G. *et al.* Novel mutations target distinct subgroups of medulloblastoma. *Nature* **488,** 43–48 (2012).
28. Korbel, J. O. & Campbell, P. J. Criteria for inference of chromothripsis in cancer genomes. *Cell* **152,** 1226–1236 (2013).

Supplementary Information is available in the online version of the paper.

Acknowledgements This research was supported as part of the St. Jude Children's Research Hospital, Washington University Pediatric Cancer Genome Project. This work was supported by grants from the National Institutes of Health (R01CA129541, P01CA96832 and P30CA021765 to R.J.G), the Collaborative Ependymoma Research Network (CERN), and by the American Lebanese Syrian Associated Charities (ALSAC). We are grateful to S. Temple for the gift of reagents and the staff of the Hartwell Center for Bioinformatics and Biotechnology, Animal Imaging Center, and Flow Cytometry and Cell Sorting Shared Resource at St. Jude Children's Research Hospital for technical assistance.

Author Contributions M.P., K.M.M., C.P., R.W., J.D.D., R.L., R.G.T., T.N.P., R.T., E.W., B.T., W.O., K.G., M.R., X.C., P.N., E.H., D.F., G.W., S.S., J.E., K.B., D.Y., B.V., H.L.M., J.B., P.G., R.H., J.M., G.S., L.D., C.L., K.O., D.Z., R.S.F., L.L.F. Yo.L., Yu.L., A.G., A.A.S., F.B. and T.M. contributed to the design and conduct of experiments and to the writing. E.R.M., R.K.W., J.R.D. and D.R.G. contributed to experimental design and to the writing. J.Z., D.W.E. and R.J.G. conceived the research and designed, directed and wrote the study.

Author Information Sequence and array data were deposited in the European Bioinformatics Institute (EBI) under accession number EGAS00001000254. Reprints and permissions information is available at www.nature.com/reprints. The authors declare no competing financial interests. Readers are welcome to comment on the online version of the paper. Correspondence and requests for materials should be addressed to R.J.G. (Richard.Gilbertson@stjude.org), D.W.E. (David.Ellison@stjude.org) or J.Z. (Jinghui.Zhang@stjude.org).

METHODS

Patient samples. Ependymomas collected under informed consent were obtained from the St. Jude Children's Research Hospital (SJCRH) tissue resource core facility and the Children's Oncology Group (COG) using protocols approved by the SJCRH and COG Institutional Review Board. Tissue samples were snap-frozen and/or formalin-fixed and paraffin-embedded (FFPE) at the time of resection. DNA and RNA were extracted from frozen tissue and peripheral blood leukocytes. Forty-one samples were submitted for whole genome sequencing (WGS), and 77 samples underwent transcriptome sequencing (RNA-seq; Supplementary Table 1). An additional 89 FFPE ependymomas were screened for structural variations (Supplementary Table 1). Criteria for submission of a tumour sample for WGS were a minimum of 5 μg of tumour DNA and a minimum of 5 μg of matching peripheral white blood cell DNA. Quant-iT PicoGreen (Invitrogen) assay was used to quantify double-stranded genomic DNA for sequencing. Basic clinical data for all patients providing tumour samples is summarized in Supplementary Table 1.

Next-generation sequencing. All methods used for library construction and WGS have been described previously (see Supplementary Information). Methods used for WGS mapping, coverage and quality assessment, single nucleotide variation (SNV) and indel detection, tier annotation for sequence mutations, prediction of deleterious effects of missense mutations, structural variations and identification of loss-of-heterozygosity have been described[27] (see Supplementary Information, and Supplementary Figs 1 and 2).

Copy number variations (CNVs) were identified by evaluating the difference of read depth for each tumour and its matching normal DNA using the novel algorithm CONSERTING (copy number segmentation by regression tree in next-generation sequencing, see Supplementary Information and Supplementary Fig. 3). Confidence for a CNV segment boundary was determined using a series of criteria, including: length of flanking segments, difference of CNV between neighbouring segments, presence of sequence gaps on the reference genome, presence of structural variation breakpoints, and any CNV in the matching germline sample. CNVs were also detected using SNP 6.0 arrays that were used as an additional quality control step for WGS (Supplementary Fig. 4).

Chromothripsis. Four criteria that define chromothripsis have been proposed recently[28]: clustering of breakpoints; randomness of DNA fragment joins; randomness of DNA fragment order; and ability to read the derivative chromosome (Supplementary Information). As randomness of DNA fragment order (the third criterion) was not entirely valid based on Korbel and Campbell's own analysis, we decided not to evaluate this feature. For all structural variations with at least one breakpoint on chromosome 11, we performed Bartlett's goodness-of-fit test for exponential distribution to assess whether the distribution of structural variation breakpoints in each tumour departs from the null hypothesis of random distribution. A significant departure from random distribution supports clustering of structural variation breakpoints. To evaluate whether there is any bias in the DNA fragment joints categorized by the structural variation types (that is, deletion, tandem duplication, head-to-head rearrangements and tail-to-tail rearrangements), we applied goodness-of-fit tests separately for inter- and intrachromosomal events with a minimum of five structural variations. A significant P value suggests biased fragment joins, which would not support chromothripsis. When both inter- and intrachromosomal data were available, we reported the lower P value to represent a more conservative assessment of the random distribution for DNA fragment joints.

RNA sequencing. Paired-end sequencing was performed using the Illumina Genome Analyzer IIx or HighSeq platform with a 100-bp read length. The resulting paired-end reads were aligned to four databases using the Burrows–Wheeler Aligner (BWA 0.5.5): human NCBI Build 37 reference sequence; RefSeq; a sequence file that represents all possible combinations of non-sequential pairs in RefSeq exons; and AceView flat file (UCSC), representing transcripts constructed from human expressed sequence tags (ESTs). After this initial mapping, final BAM files (the binary version of sequence aligment map (SAM) files) were produced by selecting the best alignment in the four databases. Structural variation detection was carried out using 'clipping reveals structure' (CREST). In addition, to identify fusion transcripts from RNA-seq we created an application called CICERO (Cicero is CREST extended for RNA optimizations), a local assembly based method that utilizes unmapped and soft-clipped reads. CICERO assembles reads around breakpoints and maps the contig to the genome to find structural variations at the transcription level. CICERO is able to find fusions with low expression, fusions within repetitive regions, fusions with a short first exon, and complex fusions involving more than two genes.

Validation of genetic alterations. A custom capture array was designed to enrich for the 18,826 high-quality SNVs (tiers 1–3) and indels and 947 structural variations discovered by WGS. This array was used to validate the presence of the non-reference allele in tumour DNA and its absence from the matched normal sample. After enrichment, samples were sequenced using Illumina technology, and resulting reads were mapped to the reference genome.

For sequences that remained uncovered we carried out independent polymerase chain reaction (PCR) amplification followed by sequencing on the MiSeq platform (Illumina). Reads were mapped as before, and 10,889 alterations were validated as somatic mutations.

RNA-seq was also used to confirm the presence of aberrant structural variation transcripts detected by DNA sequencing. PCR with reverse transcription (RT–PCR) was also used to validate the presence of fusion transcripts (see below).

Calculation of background mutation rate. The background mutation rate was calculated using validated and high-quality tier 3 mutations (that is, mutations in non-coding, non-regulatory and non-repetitive regions) normalized against all tier 3 regions with effective coverage (that is, covered by more than ten times in both tumour and matching normal samples).

Calculation of significance of structural variation position. The genome was divided into bins of 10 Mb. Breakpoint frequencies in each bin were calculated for individual samples. The enrichment of structural variation breakpoint frequency in cerebral samples was measured using the Mann–Whitney test and raw P values were adjusted using the Holm method implemented in the p.adjust function in R (version 2.11.1).

Fluorescence *in situ* hybridization. Fluorescence *in situ* hybridization (FISH) probes were derived from BAC clones (BACPAC Resources), labelled with either AlexaFluor-488 or Rhodamine fluorochromes, and validated on normal control metaphase spreads (Supplementary Table 15).

Immunohistochemistry. Immunohistochemistry was performed on both human and mouse tumours using sections (5 μm) of FFPE tissue. For detection of phospho-RELA, sections were treated to heat-induced antigen retrieval for 40 min, followed by overnight incubation with p-NF-κB p65 antibody (Ser276, bs-3543R, Bioss, 1:500 dilution). Signal detection used the Ultravision Plus detection system (Thermo Scientific). Immunohistochemistry for L1CAM was carried out using the Leica BOND-III platform (Leica Microsystems). The protocol consisted of heat-induced antigen retrieval for 20 min followed by a 15-min incubation with anti-LICAM antibody (L4543, Sigma-Aldrich, 1:100 dilution). Signal detection used the Novocastra Bond Polymer Refine Detection kit (Leica Microsystems). Immunohistochemistry for CCND1 was undertaken on the BenchMark ULTRA system (Ventana). After heat-induced antigen retrieval for 36 min, tissues were incubated for 32 min with anti-CCND1 antibody (241R-18, Cell Marque, prediluted). The ultraView Universal DAB detection kit (Ventana) was used for signal detection.

Western blot analysis. Western blot analysis was performed using standard techniques. Antibodies used included NF-κB p65 (Abcam catalogue no. ab32536; Rb monoclonal and Cell Signaling catalogue no. 4282), GAPDH (Millipore catalogue no. 374), Lamin B1 (Abcam catalogue no. ab16048), and β-Actin (CST 4967; Rb polyclonal).

RT–PCR. Transcription of fusion produces from structural variations was confirmed by RT–PCR. RNA was extracted from either snap-frozen or FFPE tumour samples, and reverse-transcribed using SuperScript VILO (Life Technologies) and the iScript cDNA Synthesis System (Bio-Rad), respectively. PCR was carried out using GoTaq Long PCR Master Mix (Promega), using specific primers (Supplementary Table 14). Fusions were confirmed by direct sequencing.

Cloning and retroviral production. Human complementary DNA clones of C11ORF95, RELA and YAP1 were cloned into the pCX4-IRES-red fluorescence protein (cRFP) vector. The Clontech In-Fusion HD EcoDry Cloning Plus system was used to generate fusion constructs. All constructs were verified by sequencing and used to make retroviruses as described previously[7]. Retrovirus-containing medium was collected, centrifuged, filtered and concentrated using Centricon plus 70-Millipore. The viral titre was determined by flow cytometric analysis of neural stem cells transduced with different dilutions of cDNA encoding retroviruses.

Fractionation of nuclear and cytoplasmic extracts. Mycoplasma-negative human 293T cells (ATCC, CRL-11268) were lysed directly on plate using 500 μl Buffer A (10 mM HEPES, pH 7.9, 10 mM KCl; 0.1 mM EDTA, 1 mM EDTA, 4% IGEPAL and 10 ug ml^{-1} of aprotinin, leupeptin and pepstatin A) for 10 min at 21°C–23°C. After high-speed centrifugation, lysates corresponding to the cytoplasmic fraction were transferred to a new tube. The pellet was resuspended by vigorous shaking at 4 °C in 150 μl buffer B (20 mM HEPES, pH 7.9, 0.4 M NaCl, 1 mM EDTA, 10% Glycerol and 10 μg ml^{-1} of aprotinin, leupeptin, and pepstatin A). After top-speed centrifugation, lysates corresponding to the nuclear fraction were transferred to a new tube. Total protein concentration was assessed by Bradford analysis and samples were prepared for western blot using equal volumes of 2× RIPA Buffer.

Promoter transactivation reporter assays. Cells were co-transfected with 6 μg of NF-κB reporter plasmid 5xkB.eGFP. Forty-eight hours later cells were stimulated, for 6 to 8 h with 5 to 50 ng ml^{-1} human TNF or vehicle only. Reporter

fluorescence was quantified by flow cytometry using a LSR II device (BD Biosciences).

Mouse RNA samples. Total RNA was extracted with TRIzol reagent (Invitrogen) and cDNA was synthesized using the SuperScript VILO cDNA Synthesis Kit (Invitrogen), according to the manufacturer's instructions. Quantitative real-time PCR was performed by using iQ SYBR Green Supermix on iCycler Real-Time Detection System (BioRad). The primer set used for C11ORF95 was 5′-GCGCTA CTACCACGACCACT-3′ and 5′-CTCCAATGCAAGGAGTAGGG-3′.

Ingenuity pathway analysis. To investigate the effect of the *C11orf95–RELA* fusion products on cell transcriptomes, we used Ingenuity Pathway Analysis (IPA) software (http://www.ingenuity.com/products/ipa) to compare gene expression profiles among cells and tumours harbouring various *C11orf95–RELA* fusions. In each analysis, only genes demonstrating a $\geq$ fourfold expression difference between data sets were included for network and transcription regulator analysis. Differential expression profiles were generated for the following four data sets using HT MG-430 p.m. Affymetrix array: mouse embryonic day 14.5 (E14.5)-NSC-derived $RELA^{FUS1}$ tumours versus parental mouse E14.5 NSCs (1,470 genes; 2,016 probe sets); mouse E14.5 NSCs transduced with $RELA^{FUS1}$ versus control-transduced NSCs (946 genes; 1,320 probe sets); mouse embryonic E14.5 NSCs transduced with $RELA^{WT}$ versus control-transduced NSCs (134 genes; 178 probe sets); mouse embryonic E14.5 NSCs transduced with C11orf95 versus control-transduced NSCs (15 genes; 18 probe sets).

Ingenuity networks were constructed by comparing differentially expressed genes from each data set to the curated Ingenuity database, which includes physical interactions and associations between genes and microRNAs derived from multiple public databases and the literature. Networks of fixed size that maximize connectivity to our gene list were constructed and ranked by inclusivity of differentially expressed genes and the number of multiply connected or 'focus genes' in the Ingenuity database. The statistical significance of networks was determined by Fisher's exact test. Log ratio data were introduced into network visualization, but were not part of the statistical model. The top ten significant networks in each data set are presented in Supplementary Table 17.

Affymetrix microarray analysis. mRNA expression profiles were generated using total RNA isolated from human and mouse tissues and the U133 Plus 2.0 and 430 v 2 microarrays, respectively (Affymetrix). Gene expression data were normalized using the MAS 5.0 algorithm. The data were then transformed and variance stabilized by addition of small factor of 20 that shrinks the effects of small numbers and then taking the natural logarithm. The median absolute difference (MAD) of these transformed signals was calculated for each probe set across all samples on each array separately within species. The data were then imported into Spotfire Decision Site and for each probe set and subject *z*-scores were calculated by computing the mean and standard deviation across subjects within each probeset. Differences in gene expression between defined groups (for example, control transduced versus $RELA^{FUS1}$-transduced NSCs) were defined using a series of Welch *t*-tests as described[7]. The resultant lists of *P* values were used to define probesets that passed the Bonferroni threshold at 0.05 per cent. Targets of NF-κB signalling were identified from a compilation of NF-κB target genes that is derived from the Gilmore NF-κB transcription factors website (http://www.bu.edu/nf-kb/gene-resources/target-genes/; T. D. Gilmore), and additional searches with PubMed.

Additional statistical considerations. We demonstrated previously that mock transduced NSCs do not form tumours in mice, and that a cohort size of 15 mice is adequately powered to detect a tumour incidence of 10% in mice implanted with oncogene transduced NSCs[6]. Therefore, 15 mice were each transplanted with NSCs harbouring the indicated fusion construct, or single partner gene. As no intervention was applied to animals following cell implantation, no randomization of animals or blinding of investigators was performed.

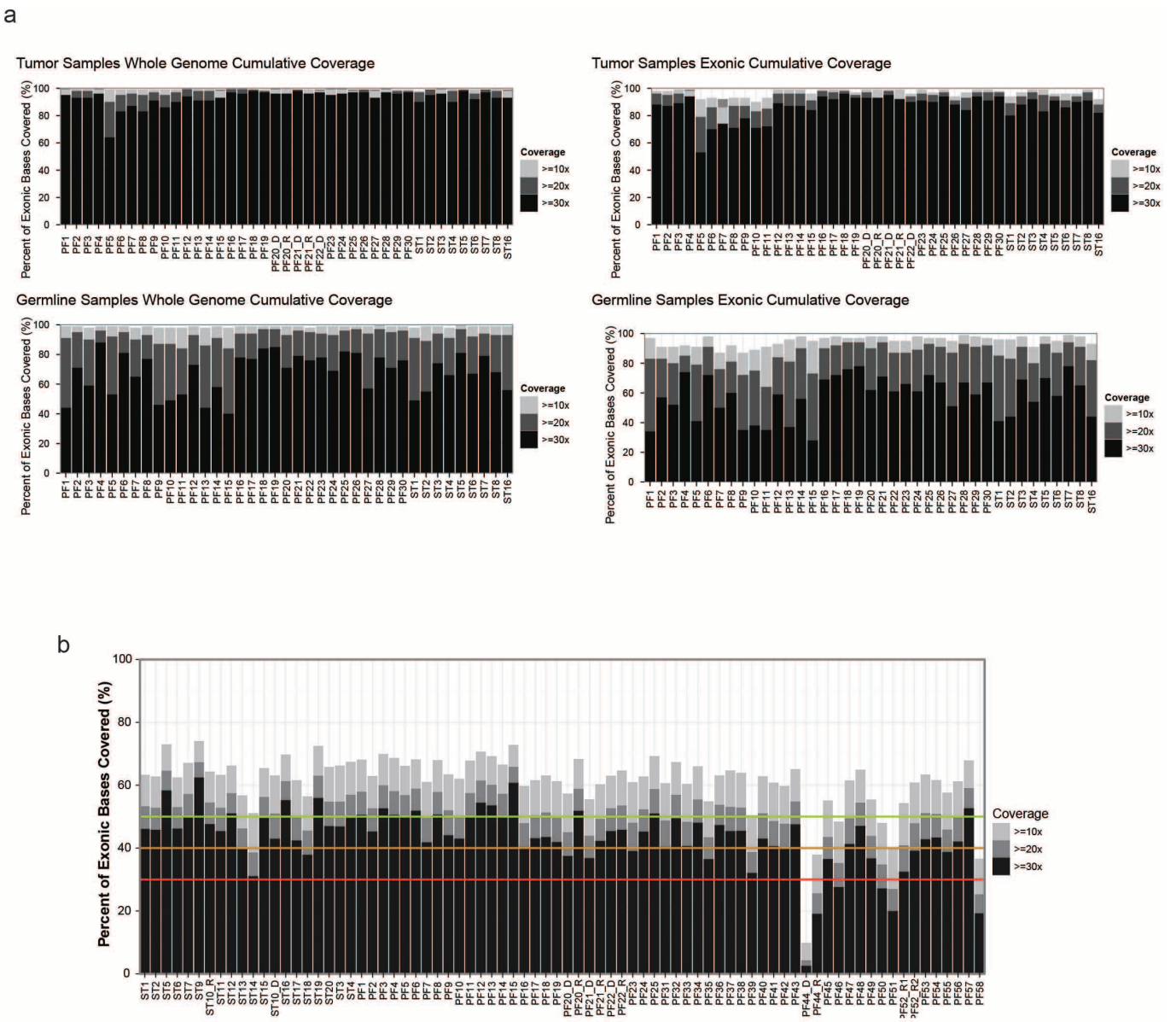

Extended Data Figure 1 | Next-generation sequencing coverage of ependymoma samples. **a**, Coverage for whole-genome sequenced cases. Percent of the genome (left) and exome (right) covered at 10×, 20× and 30× depth in tumour and germline samples. **b**, RNA-seq coverage. Coverage below the red line is considered poor quality; those with 20× depth, above the green line, are considered very high quality.

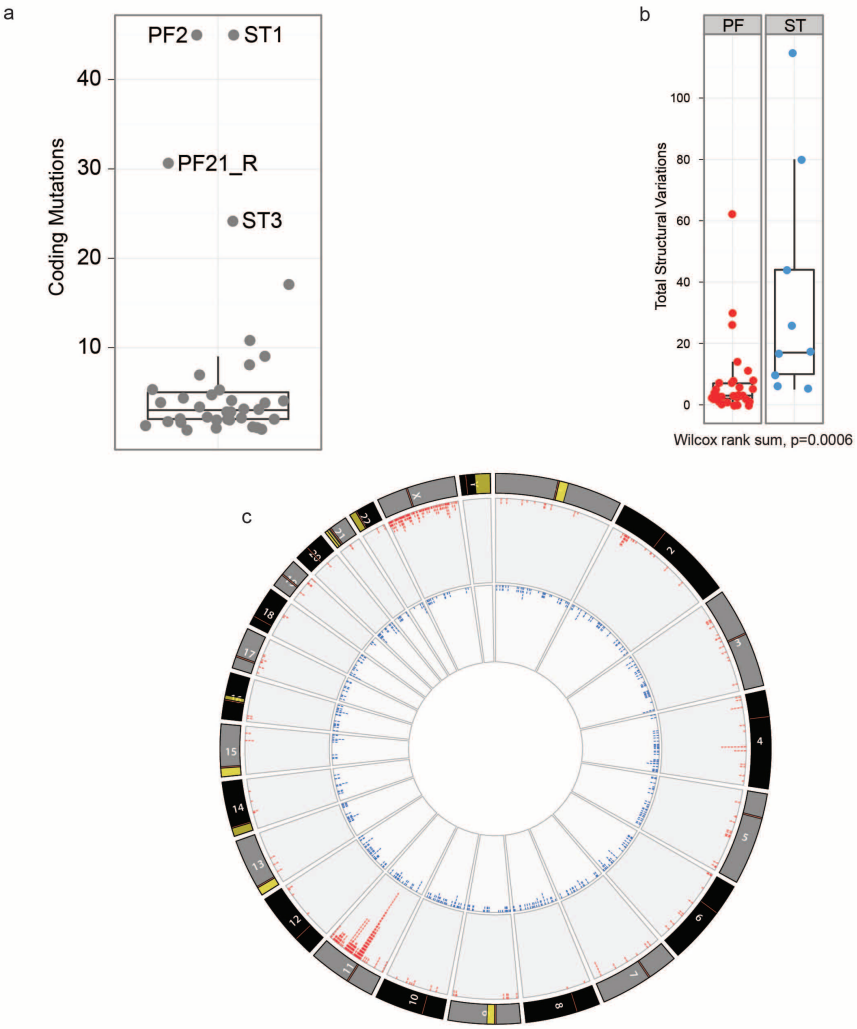

Extended Data Figure 2 | Comparison of genomic aberrations among ependymomas analysed by whole genome sequencing. **a**, The large majority of ependymomas have less than ten coding SNVs. Samples with more than 20 coding SNVs and their corresponding sample number from Fig. 1 are shown. **b**, Comparison of total number of structural variations in posterior fossa and supratentorial (ST) samples (Wilcox ranked sum test, $P = 0.0006$). **c**, Circos plot depicting SVs discovered across all supratentorial (red, outer plot) and posterior fossa (blue, inner plot) ependymomas. Each dot represents a validated or putative SV breakpoint detected by CREST in the WGS discovery cohort. Note the highly focal clustering of SVs on Chr11q in supratentorial ependymomas.

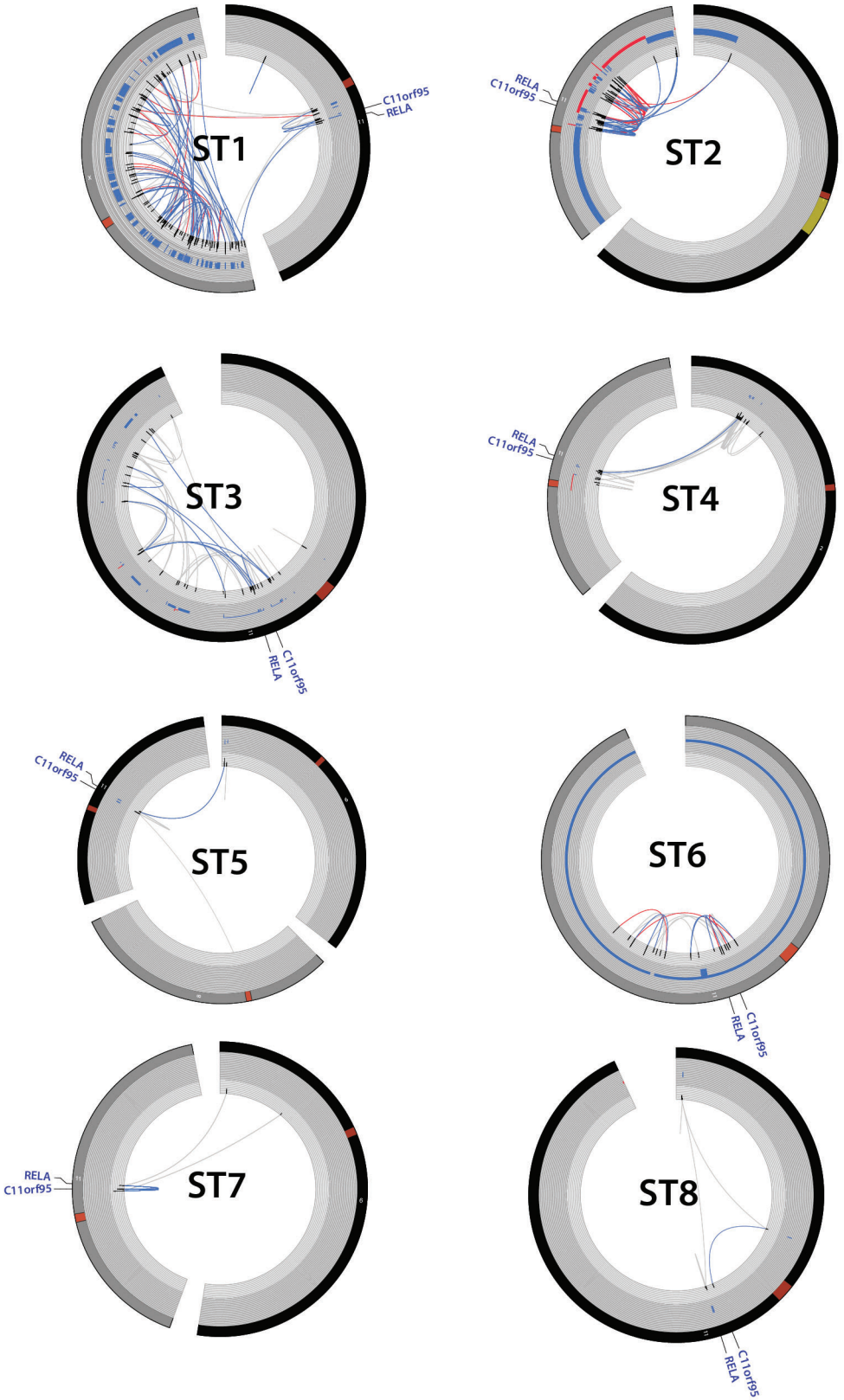

Extended Data Figure 3 | Chromothripsis in supratentorial ependymomas resulting in C11orf95–RELA translocations. Circos plots for the eight supratentorial (ST) ependymomas analysed using WGS that contained C11orf95–RELA translocations (sample numbers as Fig. 1). From the outer ring to the inner ring: chromosome, CNV calls, softclip count histogram, SVs (red, both sides with ≥10 softclips; blue, one side with >10 softclips; grey, <10 supporting softclips on either side).

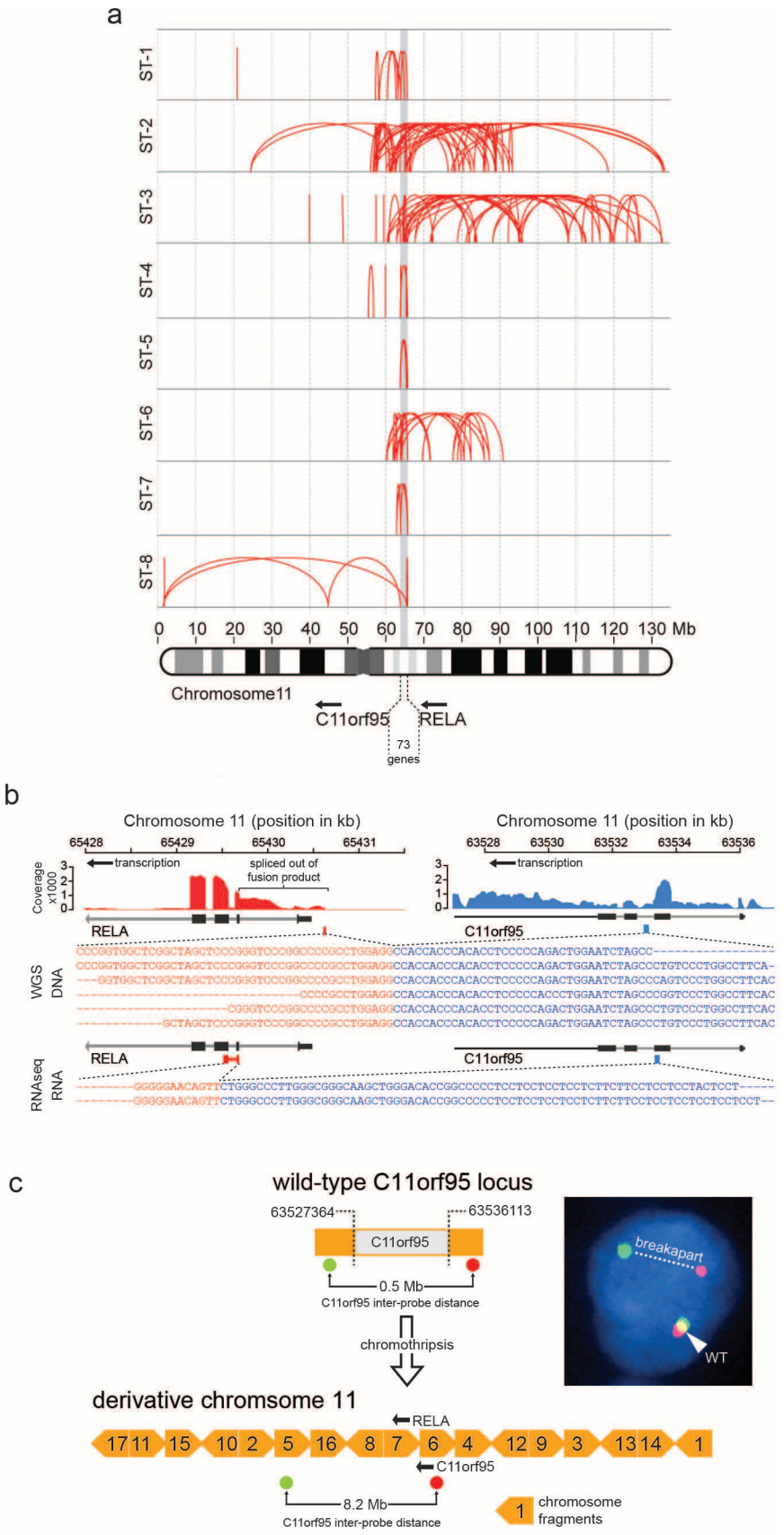

Extended Data Figure 4 | C11orf95–RELA translocations. **a**, Breakpoints of structural rearrangements (red loops) at 11q13.1 in tumours ST1 to ST8. **b**, Exemplary C11orf95–RELA translocation and fusion transcript in sample ST5. Top, RNA-seq coverage; middle, DNA sequence across the fusion breakpoint; bottom, RNA sequence. **c**, Derivative chromosome generated by chromothripsis in tumour ST6 highlighting the locations of C11orf95 'break-apart' FISH probes. Yellow block arrows represent chromosome fragments rearranged by chromothripsis. Numbers indicate fragment order on normal chromosome 11. FISH result, right. Arrows, transcription orientation.

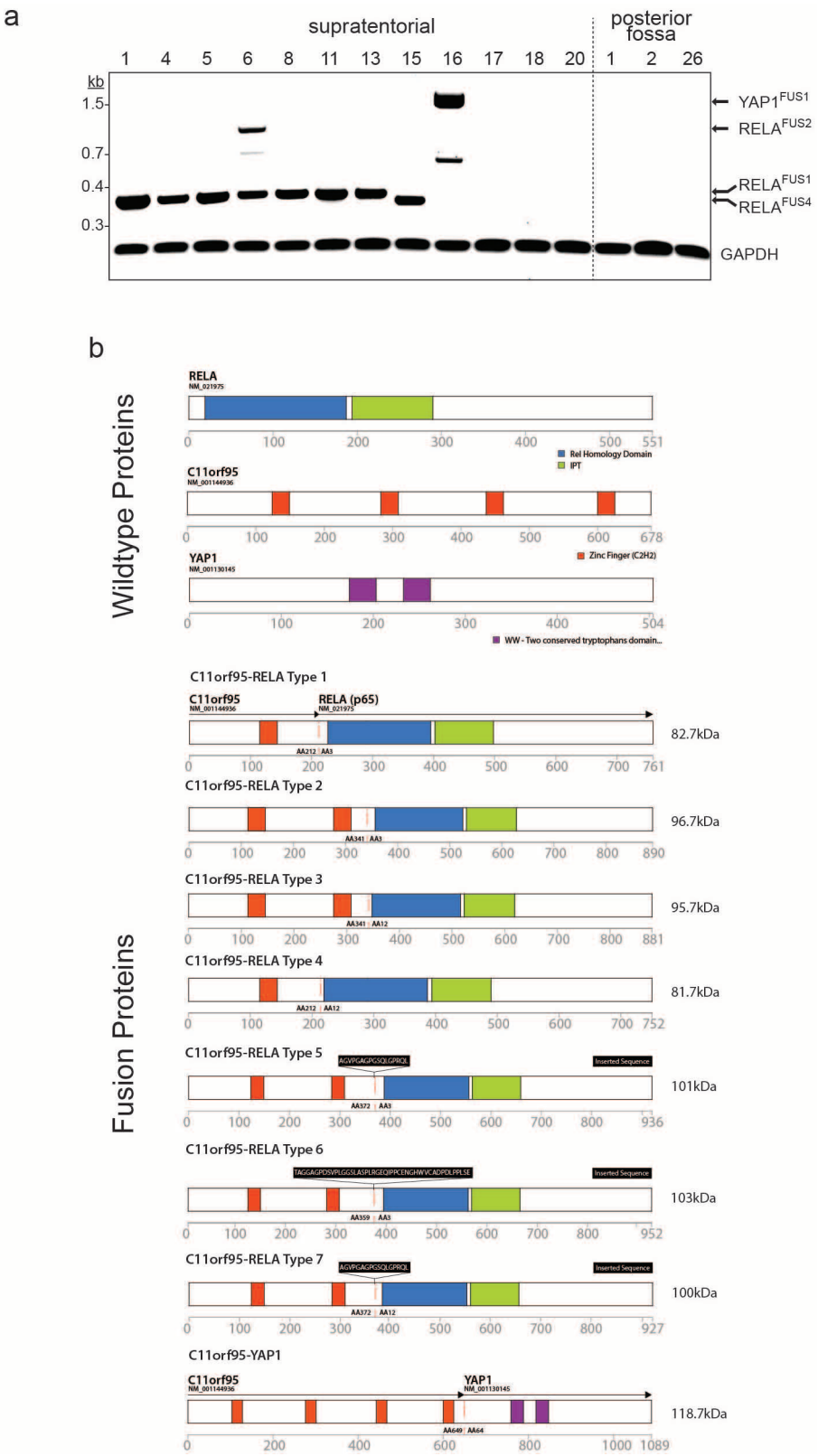

Extended Data Figure 5 | Translocation fusions: transcripts and predicted protein products detected in ependymoma. **a**, Reverse transcription PCR products of the indicated transcripts detected in tumour samples (sample numbers as in Fig. 1a). **b**, Predicted protein products of wild-type translocation partners (top) and fusion products (bottom).

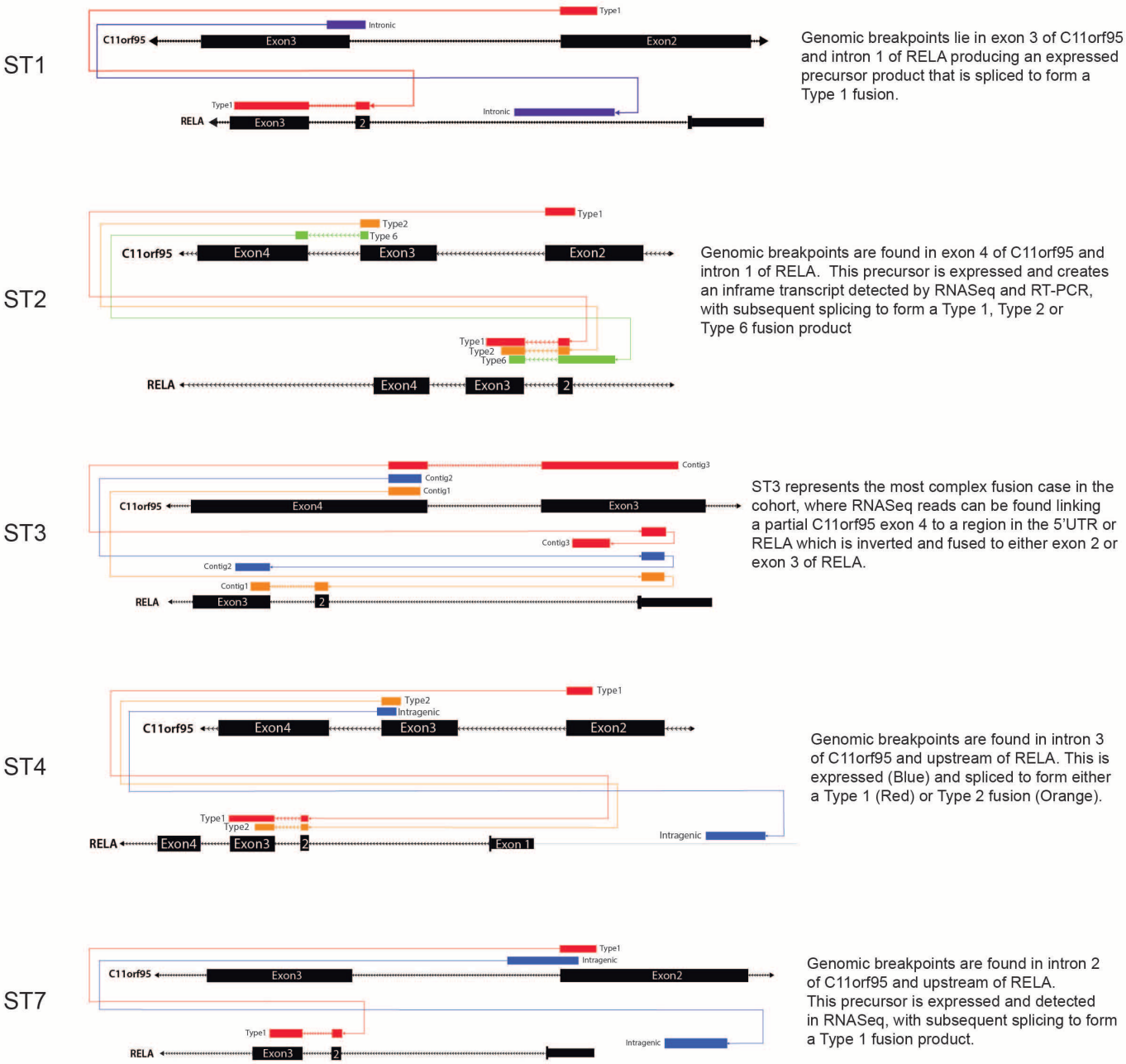

Extended Data Figure 6 | Maps of fusion *C11orf95–RELA* products. RNA-seq contig maps demonstrating the various fusion products generated through splicing of the primary C11orf95–RELA translocation transcript.

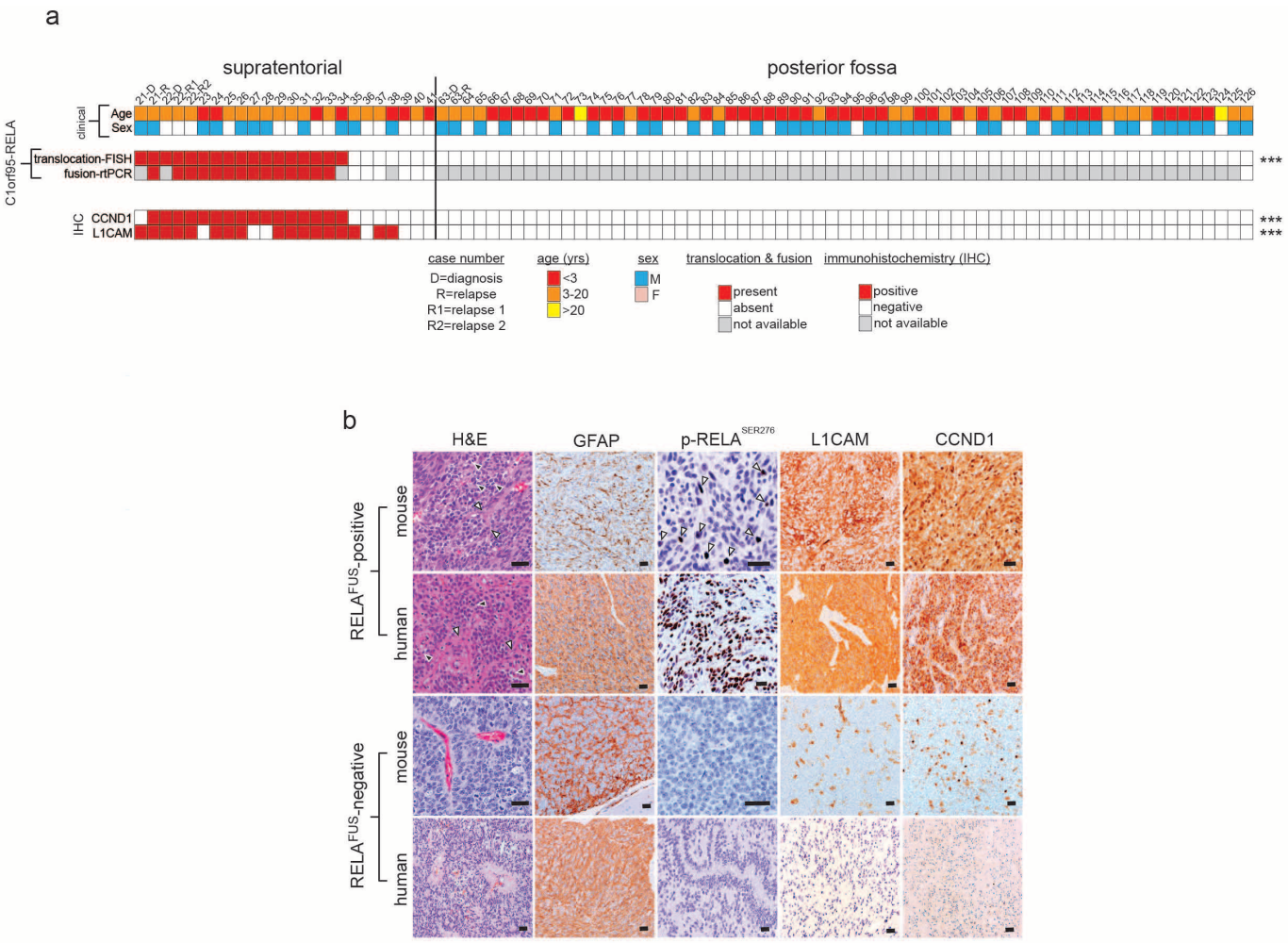

Extended Data Figure 7 | Analysis of C11orf95–RELA translocation and expression in formalin-fixed paraffin-embedded human and mouse ependymoma. **a**, Formalin-fixed paraffin-embedded (FFPE) cohort (top) and results (middle) of break-apart FISH and RT–PCR analysis of the C11orf95–RELA translocation and transcript, respectively. Tumours with 'unavailable' data had insufficient material for analysis. **b**, GFAP, p-Ser276-RELA, CCND1 and L1CAM immunohistochemistry in human and mouse $RELA^{FUS1–7}$-positive and -negative cases. The mouse tumours recapitulate the 'vascular-variant' of human supratentorial ependymoma (see haematoxylin and eosin (H&E) images). This subtype is characterized by a branching network of capillaries (white arrows) and cytoplasmic clearing (black arrows). $***P < 0.0005$. Scale bar, 50 μm

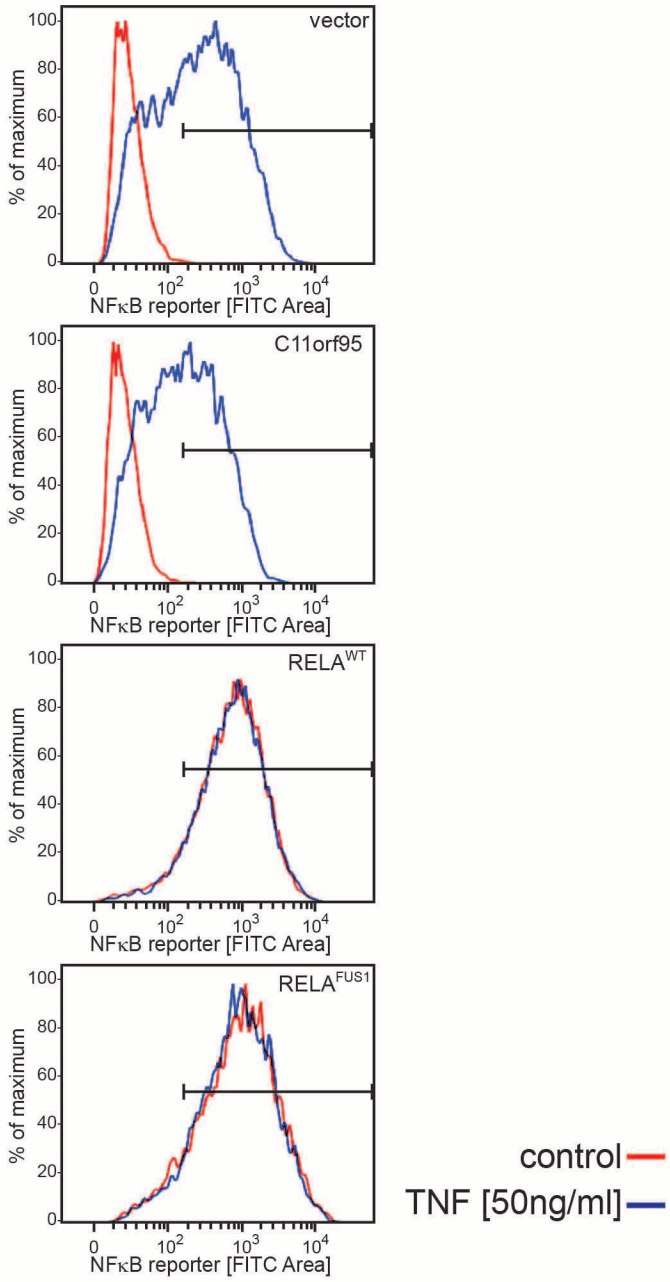

Extended Data Figure 8 | C11orf95–RELA fusion protein spontaneously activates an NF-κB transcriptional reporter. NF-κB–green fluorescence reporter (GFP) activity in 293T cells transduced with the indicated virus, treated for 60 min with TNF (50 ng ml^{-1}) or vehicle control.

CORRIGENDUM

doi:10.1038/nature13299

Corrigendum: C11orf95–RELA fusions drive oncogenic NF-κB signalling in ependymoma

Matthew Parker, Kumarasamypet M. Mohankumar, Chandanamali Punchihewa, Ricardo Weinlich, James D. Dalton, Yongjin Li, Ryan Lee, Ruth G. Tatevossian, Timothy N. Phoenix, Radhika Thiruvenkatam, Elsie White, Bo Tang, Wilda Orisme, Kirti Gupta, Michael Rusch, Xiang Chen, Yuxin Li, Panduka Nagahawhatte, Erin Hedlund, David Finkelstein, Gang Wu, Sheila Shurtleff, John Easton, Kristy Boggs, Donald Yergeau, Bhavin Vadodaria, Heather L. Mulder, Jared Becksfort, Pankaj Gupta, Robert Huether, Jing Ma, Guangchun Song, Amar Gajjar, Thomas Merchant, Frederick Boop, Amy A. Smith, Li Ding, Charles Lu, Kerri Ochoa, David Zhao, Robert S. Fulton, Lucinda L. Fulton, Elaine R. Mardis, Richard K. Wilson, James R. Downing, Douglas R. Green, Jinghui Zhang, David W. Ellison & Richard J. Gilbertson

Nature **506,** 451–455 (2014); doi:10.1038/nature13109

In this Article, author Jared Becksfort's surname was incorrectly spelled 'Becksford'. Also, his affiliation should be the Department of Computational Biology and Bioinformatics (not the Department of Pathology) at St Jude Children's Research Hospital. His name and affiliation have been corrected online.